Progress in Nuclear Energy 166 (2023) 104976

Contents lists available at ScienceDirect

Progress in Nuclear Energy

journal homepage: www.elsevier.com/locate/pnucene

Parametric study of molten core concrete interaction and assessment of corium coolability in the light of MCCI experiments☆

Nasir Hayat Hengra [a,*], Chang Hyun Song [b], Sung Joong Kim [b], Muhammad Ilyas [a]

[a] Department of Nuclear Engineering, PIEAS, Pakistan
[b] Department of Nuclear Engineering, Hanyang University, South Korea

ARTICLE INFO

Keywords:
Light water reactor
Corium concrete interaction
Water ingression
Melt eruption
MELCOR 2.2

ABSTRACT

Molten Corium Concrete Interaction (MCCI) is an important phenomenon observed in the late phase of reactor severe accidents. A realistic analysis of MCCI can save cost and efforts to mitigate severe accidents. The heat transfer mechanisms in MCCI, such as melt eruption and water ingression, are the primary focus of current research owing to complications in their quantification and replication in severe accident analysis codes. This study investigated MCCI using top flooding strategy with MELCOR 2.2 code for two concrete types, and three experiments that were conducted under (OECD/MCCI-1 program). The results demonstrated that the ablation process terminated in the case of Limestone Common Sand (LCS) concrete. In the simulation of siliceous (SIL) concrete, the maximum and average melt front locations confirmed the asymmetrical ablation progression. The LCS concrete showed a smaller axial ablation front in this study; however, the comparison with the concrete ablation volume (0.21 m^3) showed an exact match, and the difference between the experimental and predicted ablated mass of concrete was only 0.61%. The quantitative comparison between the prediction of the present study, CORQUENCH code, and experimental results is provided. The parametric values of MCCI phenomenon are also predicated and model improvement for MELCOR 2.2 code are discussed as well.

1. Introduction

1.1. MCCI phenomenon

Molten corium concrete interaction (MCCI) is a significant phenomenon that occurs during severe accidents in nuclear power plants, particularly in the late phase. The process involves the ablation of cavity concrete due to the attack of high-temperature corium that flows out of the reactor pressure vessel (Farmer et al., 2009). The physical and chemical decomposition of concrete caused by the corium, along with the decay heat generated by fission products, exothermic oxidation of metals, and released gases from concrete, expedite the ablation progression, leading to a weakening of the basemat's structural strength (Eppinger et al., 2000). The generation of non-condensable gases (NCGs) from decomposition of concrete rises the pressure of the containment and the concentration of flammable gases, thereby posing a significant threat to containment integrity, which is the last safety barrier against fission product release. Current understanding of corium concrete interaction (CCI) suggests that numerous parameters influence the ablation process, with significant uncertainties existing in these parameters (Christophe et al., 2010). The critical parameters that influence the termination of the concrete ablation are corium conditions, concrete type, presence of water, and cavity geometry (Hengra et al., 2023). Fully or partially oxidized corium conditions impact the heat transfer to the concrete, with light metal melts (zircaloy/steel) having slightly higher temperatures than the liquidus temperatures of concrete (Kim et al., 2019). The addition of concrete content to the corium mixture reduces the temperature, causes variations in physical properties, and decreases heat transfer to the concrete and cavity surface (Amidu and Addad, 2022). Different concrete types possess varying constituents, carbonate (gas) content, and corresponding thermal properties that affect the cavity heating rates, ablation rates, and crust formations (Kevin et al., 2014). Each concrete type has a specific ablation enthalpy and specific solidus, liquidus, and ablation temperatures. Crust formation between the corium mixture and concrete surface may impede the concrete ablation, which may occur in the early phase of CCI (Amidu and Addad, 2022).

Water injection, as a mitigation measure, affects the heat transfer

☆ The first and second authors contributed equally as the co-1 st author.

* Corresponding author.
E-mail addresses: nasirhayat_18@pieas.edu.pk, chemist042004@gmail.com (N.H. Hengra).

https://doi.org/10.1016/j.pnucene.2023.104976
Received 18 March 2023; Received in revised form 3 October 2023; Accepted 13 November 2023
Available online 24 November 2023
0149-1970/© 2023 Elsevier Ltd. All rights reserved.

and ablation mechanisms of CCI. The addition of water promotes crust formation between the water and melt mixture. This crust may stop water percolation to below corium mixture or a gap is created below crust, which may delay the termination of ablation (usually in the late stage of CCI) (Yeo and No, 2019). The location of water injection, whether from the upper side (top flooding), the bottom side, or laterally, has different effects on the ablation process. The cavity geometry also plays a crucial role, with any changes in the heat transfer area affecting the ablation lengths. Further research and analysis are necessary for a better insight of these phenomena (Sevon, 2005), (Journeau et al., 2018).

The development of physical models for the parameters influencing the CCI progression and a better understanding of the process and its termination requires both theoretical and experimental studies. Precise determination of heat transfer coefficients and analysis of the heat transfer mechanisms from corium to concrete are needed. Additionally, the assessment of water coolability issues in cavities for different concrete types and corium melts is necessary for better mitigation of severe accidents (Journeau et al., 2018).

1.2. Literature review and previous studies

Over 50 experimental investigations have been conducted to understand severe accidents and safely mitigate them, including investigations of simulant and prototypic materials, such as fuel rod material. Of these experiments, over thirteen have been carried out using uranium oxide as a prototypic material. Several facilities that perform severe accident research, including research on the CCI phenomenon, have been reviewed (Sevon, 2005) (Christophe et al., 2010). Here is a list of experiments in Table 1 performed during past along with their specifications. Based on the findings of these experiments, heat transfer correlations were drawn, and numerical models were established and validated in the simulation codes (Sevon, 2005).

The Melt Attack and Coolability Experiments (MACE) initiated for understanding of phenomenon involved in MCCI. Quantification of MCCI phenomenon performed through Melt Coolability and Concrete Interaction (MCCI-1), and MCCI-2 test programs using prototypic melts with different concrete and water injections. The results of these experiments provided conclusive findings related to the potential heat transfer mechanism during CCI. The MCCI-1 tests (CCI-1 to CCI-3) showed that there exists a substantial disparity between the ablation behaviors of different concrete types (Farmer et al., 2006). Under the MCCI-2 program, a different set of conditions than the MCCI-1 program was used to conduct another set of three experiments, CCI-4 to CCI-6. These tests provided confirmatory evidence of code predictions and a better understanding of two-dimensional CCI under dry and wet conditions (Farmer et al., 2010). A recent MCCI related experimental study using simulant with cylindrical geometry has been conducted by Xu et al. (Xu Zhang et al., 2022). High costs are involved for prototype CCI experiments. Alternative to this, supplementary comparative studies of simulations and experiments can significantly decrease MCCI uncertainties.

In terms of code simulation and its development, several research studies related to MCCI utilizing specialized codes and numerical methods have been conducted (Penghui et al., 2017). The moving particle semi-implicit (MPS) method is a numerical method which is effectively used for MCCI and ablation pattern determination (Chai et al., 2017). In the research of MCCI, the particle methods have been widely employed, and they have revealed several mechanisms about MCCI (Li and Yamaji, 2016). Improved MPS methods are used for crust effects on transient MCCI (Cai et al., 2020a,b) and erosion rate prediction of EPR sacrificial material (Li et al., 2017).

Computational studies have highlighted the role of melt eruption (ME) and water injection (WI) as heat transfer mechanisms during CCI (Farmer et al., 2001). A study by Kevin et al. (2014) compared the results of the Fukushima plant cavity (1F1) using three codes: MELCOR (Humphries et al., 2021a), MELTSPREAD (Farmer, 2017), and CORQUENCH (Farmer, 2018). The study observed that the MELCOR 2.1 code requires several upgrades, especially in the cavity package to accurately model the MCCI and account for the WI and ME. Another simulation of MCCI-1 experiments, CCI-2, CCI-3, and CCI-6, were performed with the COREQUENCH code, and the validation studies conducted in the presence of NCGs showed that several modifications in heat transfer correlations are required (Farmer, 2018). The Epstein's WI model (Epstein, 2006) is presently used by default within the system of equations for debris/pool to improve the MELCOR code cavity package, resulting in an increase in predicted heat transfer from debris surface to water (Humphries et al., 2021a).

The MELCOR 2.2 code packages incorporate several models, including the ME and WI models (Sevon, 2017) (Humphries et al., 2019), which are designed to assess erosion in the cavity and the coolability of the melt concrete mixture. These models have been tested through a series of prototypic experiments as discussed above. To ensure the accuracy of the MELCOR code, various studies have been conducted to validate and verify its performance in CCI experiments. One such study, carried out by Kim et al. (2005), used scaling methodology to account for geometric differences between the MELCOR code (Cylindrical) and the CCI-2 experiment (rectangular shape). The results revealed that MELCOR 1.8.5 predicts higher radial and axial ablation

Table 1
Description of experimental facilities, composition of test material, and other details.

Name of facility	Type of material used	Details
BETA experiments (1984–1992) (Alsmeyer et al., 1995)	LCS/SIL Concrete, 1800–2300 °C melt	Axial/radial erosion rates and the effect of input power was studied
KAJET (1999–2002) effect (Huber et al., 2005)	Melt of Al_2O_3 and iron (Fe) on SIL and Boro-Silicate Glass (BSG) concrete	Heat transfer by Jet impingement during CCI was studied
Kapool tests (Eppinger et al., 2000)	A melt of Al_2O_3, Fe and zirconium without decay heat using BSG and SIL concrete	Erosion rates and heat transfer coefficients for different concrete types were calculated at a stable temperature profile
TURC, SNL (Sevon, 2005)	Oxidic UO_2, ZrO_2 with/ without metallic materials (SS, Zr) with variable heating powers	The concrete ablation process was attempted for limestone and basaltic concretes
SURC, SNL (Sevon, 2005)	UO_2, ZrO_2 and Zr with LCS concrete, no decay heat	Transient heat conduction, low ablation, and early solidification of the melt was observed
HECLA-VULCANO Tests (Christophe et al., 2010)	Metallic/oxidic melt, SIL, LCS concrete with/ without decay heat	CCI cylindrical cavity and anisotropic ablation was observed for SIL
WETCOR 1, SNL, 1991 (Blose et al., 1993)	Al_2O_3, CaO, and SiO_2, with LCS concrete	Water addition was inadequate to stop the ablation progression
Melt Attack and Coolability Experiments (MACE), ANL, 1980, (Farmer et al., 2001)	Prototype materials and water injection	Four heat transfer mechanisms were discovered, bulk boiling, water ingression, melt eruption, and renewal of surface with crust break-up
Melt Coolability and Concrete Interaction MCCI-1 program, ANL, 2002–06 (Farmer et al., 2006)	Prototype materials and water injection, LCS and SIL concrete with decay heat	Quantification of four heat transfer mechanisms identified in MACE. Ablation profile for different concrete types was studied
MCCI-2, 2006–2010 (Farmer et al., 2010)	Prototype materials and water injection, LCS and SIL concrete with decay heat	Dry and wet cavity and MCCI ablation reaction mechanisms, model parameters finding and improvement

values than the CCI-2 experiment. Jung et al. (2018) conducted a sensitivity study to assess the impact of input parameters on the MCCI model parameters. MELCOR 2.2 was used to determine the effect of concrete type and delay in water injection time for tuning purposes. Cho et al. (2020) performed an uncertainty analysis of the input parameters needed in MELCOR 1.8.5 to 2.2 for the CCI-2 experiment. The results showed a significant variation in the position of the axial and radial ablation front when input parameters were altered.

1.3. Objectives

The studies mentioned previously have highlighted the importance of advanced numerical simulation models for investigating existing issues and minimizing the requirement of conducting costly experiments. The MELCOR code is an advanced engineering thermal hydraulic code that has been consistently upgraded based on experimental and theoretical studies. The MELCOR 2.1 code version includes significant modifications related to the cavity package, while MELCOR 2.2 incorporates models for WI, ME, heat transfer, and property evaluation based on recommendations from CCI experiments and numerical/simulation studies (Sevon, 2017) (Humphries et al., 2019). However, it was confirmed that further investigation and improvement of MELCOR model is needed because the prediction results were quite different with experimental findings. Therefore, one of the objectives of present study is to investigate CCI experiments with the MELCOR 2.2 code, and provide suggestions for the next revision of the code. This study aims to bridge gaps in the existing literature and serve as a benchmark for future applications in reactor cavity designs and interpretation of experimental results.

The present study aims to obtain detailed and accurate information about additional parameters (mass and heat transfer) that were not available in previous experiments and numerical studies. The study will investigate melt stabilization using the top flooding strategy and evaluate ablation, temperature, and heat transfer processes occurring in different types of concrete. Additionally, the study will investigate the termination of ablation progression using the top flooding approach, which is crucial for severe accident management. Finally, the study will assess the models used in MELCOR 2.2 and quantify the improvement in heat transfer from the ablated corium–concrete mixture.

Analysis methodology is discussed in Section 2 and results and discussions are provided in Section 3. The summary and conclusions are presented in Section 4, and the references are included in Section 5.

2. Analysis methodology

The MELCOR input model is developed for CCI experiments 1–3 in this study. The experimental conditions, such as the compositions of corium and concrete, were obtained from the information described in experiment report (Farmer et al., 2006). The introduction of code, numerical models, and experimental specifications are provided in the following subsections.

2.1. Analysis scheme of MELCOR code

MELCOR is an advanced engineering-level analysis code which emulates the overall accident progression in nuclear power plant. MELCOR has number of modules to simulate a variety of transients in light water reactors. The thermal-hydraulic behaviors in the reactor coolant system, secondary system, reactor cavity, and containment building can be modeled. For core degradation inside the RPV, models for the core heat-up, melting, and corium relocation exist. In terms of core-concrete interaction, ablation of concrete, resultant hydrogen production, transport, and combustion inside the containment building can be predicted. Ultimately, the release and transport of fission products is calculated. Therefore, MELCOR is utilized to estimate source term under severe accident situations in many previous studies (Humphries et al., 2021a).

In the experiment, it was confirmed that there are certain phenomena, such as ME and WI, which have a significant effect on overall heat transfer during MCCI. In other words, it implies that it should be appropriately simulated in code for accurate prediction. Accordingly, the ME and WI models are developed in MELCOR 2.2 code based on proposed correlations obtained from the experimental results (Humphries et al., 2019), (Humphries et al., 2021b). These models should be validated and improved for further realistic prediction.

2.1.1. Heat transfer model

The heat flux to concrete is dependent on the properties of the concrete such as the density, and decomposition enthalpy per unit mass of concrete as well as on the area of the eroding concrete with erosion velocity. Especially, the erosion velocity is determined by the heat flux, which is based on the temperature difference between the corium and interface, and the heat transfer coefficient at the interface.

The melting temperature of the concrete is determined based on the composition of the concrete. The conductive heat transfer from the melt front to the intact concrete is ignored due to the poor thermal conductivity of concrete. The interfacial temperature is determined through correlation based on experimental results, and it requires discreet evaluation because of the high uncertainty in its values (Sevon, 2005).

The heat transfer coefficient is determined based the Nusselt number (*Nu*) during MCCI process. *Nu* is determined by the specific correlations that rely on the Rayleigh number (*Ra*) and the Prandtl number (*Pr*). The values of material properties depend on the melt and concrete interface temperatures. These properties are used to calculate *Nu*, *Ra* and *Pr* numbers though correlations i.e. surface correlation proposed by Incropera et al. (IncroperaDeWitt, 2002).

For cases with sufficient gas generation by concrete decomposition, the correlation proposed by Green et al. (Greene, 1991) is used for prediction of bubble heat transfer coefficient for both horizontal and vertical sides. Additionally, the modified Kutateladze correlation (Bradley et al., 1993) for the bubbling heat transfer coefficient in the Bradley-CORCON model is used in CORCON-Mod-3 code, and the same is applied in the MELCOR code in the revised form (Humphries et al., 2021a). The initial viscosity calculated is enhanced by using the Kunitz and Ramacciotti multipliers.

2.1.2. Water ingression models

Water ingression can occur when the initially dry reactor cavity is filled by water after corium pouring. At the interfacial surface between the corium and overlying coolant, there are crack in the crust. Accordingly, the coolant can be introduced into the ablation zone through these cracks, which increase the heat removal rate, resulting in direct cooling of the corium concrete mixture (Farmer, 2018).

Previously, there is no model in MELCOR code so that MCCI was predicted conservatively without heat transfer via direct cooling (Farmer et al., 2009). For deriving an analytical model for water ingression, experimental studies were carried out such as SSWICS test to assess the effect of water ingression (Lomperski and Farmer, 2007) (Nayak et al., 2009) (Yeo, 2018). Based on experimental results analytical models were developed for accurately predicting the process of heat transfer due to the water ingression.

WI model incorporated in MELCOR code 2.2, is a major modeling improvement from its previous versions. It predicts the heat transfer and mass transfer rates from the melt–concrete mixture to the surface and interface. It is applied with the presence of water and gases which are penetrating the crust surface as shown in Eq. (1) (Humphries et al., 2021b).

$$q''_{dry} = C_{dry}\left[\left\{\frac{h_{lv}(\rho_l-\rho_v)g}{\nu_v}\right\}^5 + \left\{\frac{N_{dry}k_{cr}^2\Delta e_{sat}^2}{C_p\Delta e_{cr}}\right\}^4\right]^{1/13}\{\alpha_T(T_{cr}-T_{sat})\}^{15/13} \quad (1)$$

q''_{dry} is dry out heat flux, C_{dry} is an empirical constant, h_{lv} is the heat of

vaporization of water, ρ_l is the density of water (kg/m^3), ρ_v is the density of steam (kg/m^3), g is the gravitational constant (9.81 m/s^2), ν_v is the dynamic viscosity of steam, N_{dry} is a numerical constant (0.1 K-m$^{1/2}$), K_{cr} is the thermal conductivity of crus, ∇e_{sat} is the change in specific enthalpy from melt temperatures to saturation temperature, C_p is the specific heat capacity of melt, α_T is the coefficient of thermal expansion for melt (1/K), T_{cr} is the crust temperature calculated with Eq. (2), and T_{sat} is the saturation temperature of steam.

$$T_{cr} = T_s - \frac{\sigma_{tens}}{\alpha_T E} \tag{2}$$

σ_{tens} is the tensile strength of the crust (6.77E7 Pa), and E is Young's modulus for the crust (1.25E11 Pa). The thickness of the crust, δ_{cond}, can be determined (Humphries et al., 2021b) with Eq. (3).

$$\delta_{cond} = K_{cr}\frac{(T_B - T_{Sat})}{q''_{dry}} \tag{3}$$

2.1.3. Melt eruption model

The additional heat transfer could happened during MCCI if decomposing material come out at the surface of cavity covered with water. The produced gases by the decomposition of concrete sparges out of the cracks in the crust surface after flooding. When sparging gases have sufficient velocity to entrain the melt particle, mass and heat transfer occurs through entrainment as a result of melt droplets movement to the crust surface (Amidu and Addad, 2022).The melt entrainment rate is determined by volumetric flow rate of internal gas and the melt entrainment coefficient (Farmer, 2018), (Kim et al., 2019). MELCOR 2.2 has melt eruption model in its CAV package as follows. The mass transfer from the melt layer to the debris layer is based on specific criteria, which depends on the entrainment coefficient and gas sparging rate, as shown in Eq. (4).

$$j_{melt} = k_{ent}\, j_{gas} \tag{4}$$

j_{melt} is the melt ejection rate (m/s), j_{gas} is the gas sparging rate (m/s) and k_{ent} is the entrainment coefficient calculated from the Ricou–Spalding correlation using Eq. (5).

$$k_{ent} = E_{ent}\left(\rho_{gas}/\rho_{melt}\right)^{1/2} \tag{5}$$

E_{ent} is the entrainment constant (default value: 0.06), ρ_{gas} is the gas density (kg/m^3), and ρ_{melt} is the melt density (kg/m^3). The criterion of melt ejection is based on the minimum gas sparging rate (j_{min}), which is calculated based on the following correlation using Eq. (6).

$$j_{min} = k_{prm}\frac{(\rho_{cr} - \rho_m)g}{\mu_g} \tag{6}$$

ρ_{cr} is the crust density (kg/m^3), μ_g is the gas viscosity (Pa-s) , *and* k_{prm} is the permeability of crust calculated based on the Jones correlation as shown in Eq. (7).

$$k_{prm} = \frac{2\mu_v q''_{dry}}{\rho_v h_{lv}(\rho_l - \rho_v)g} \tag{7}$$

h_{lv} heat transfer coefficient (W/m^2-k), ρ_l is the liquidus phase density, ρ_v is the vapor-phase density, q''_{dry} dry out heat flux (W/m^2) (Humphries et al., 2021b).

2.2. CORQUENCH code

The CORQUENCH code has been developed as a simple modular MCCI analysis tool consisting of melt/water heat models to compare results with experiments. It includes the multi nodal analysis capability with its water inventory model for more realistic evaluation of cavity flooding. A transient concrete ablation model at the interface of concrete/melt is used for heat transfer based on integral thermal boundary layer (Farmer, 2018). It has capability to model rectangular geometry and insulate certain surfaces (Kevin et al., 2014). Water ingression model is included in CORQUENCH code. The water ingression model is different in MELCOR and CORQUENCH code due to parametric differences although both have same mathematical models (Sevon, 2017).

2.3. Experimental setup and simulation

CCI tests were performed using a test apparatus in which the prototypic melt was placed inside the test concrete. Various measurement devices were embedded in the concrete for measurement of major thermal-hydraulic values. The heat is generated by direct electrical heating (DCH) for emulating decay heat generation. Furthermore, other systems such as data acquisition system (DAS), electrical power supply, two steam condensation tanks, water supply, and an off-gas system to filter and vent the off-gases were provided (Farmer et al., 2004a,b).

The main part of the test section, as shown in Fig. 1, consisted of concrete test blocks of 50 cm × 50 cm. The total height of the test section was approximately 3.4 m. The prototypic melt ingot (25 cm depth and 50 cm length/width) has been produced by the thermite reaction, which was poured into a concrete block with an initial dimensions of 25 cm × 50 cm to hold the melt, as shown in Fig. 2. The maximum ablation limit was set at 35 cm from the available 50 ± 5 cm in both of radial and axial directions to ensure safety. The test specifications for the CCI 1–3 tests are summarized in Table 2. For the CCI experiments, two types of concrete were used. The CCI-1 and CCI-3 tests were conducted with Silicious (SIL), and CCI-2 tests were performed with limestone common sand (LCS) concrete. Chemical composition of concrete used in experiment is given in (Farmer et al., 2006) and same employed in simulations. The CCI tests utilized a prototypical PWR melt that initially comprised with a small amount of concrete. For CCI-1–3, the corium melt ingot contained 8 wt% or 15 wt% of concrete, as presented in Table 3. There were specifically built 2-dimensional concrete test pieces with dimensions of 50 × 50 × 50 cm. Especially, for radial direction, two sides of the square-shaped test section were insulated (Farmer et al., 2005a,b).

Due to variations in reaction completions, thermite reactions produce slightly different masses and compositions of melt ingot in each test. Once poured into the test section, the cavity concrete is ablated by the melt. Decay heat (DEH) rate was specified at 150 kW in CCI-1 and 120 kW in CCI-2 and CCI-3 and achieved within 60 s after pouring of the melt. The dry cavity condition is maintained until the water addition, as mentioned in Table 2. The DEH gradually decreased in CCI-2 and CCI-3 after water addition until data acquisition was stopped; however, water was added in CCI-2 at 5.5 h after occurrence of corium-concrete interaction and radial ablation depth reached 30 cm.

A rapid reaction occurred between the melt and the concrete after the initial crust was broken up, which leading to the direct contact. The inclusion of concrete into the corium resulted in a decrease in melt temperature. The water addition caused most of decay heat to be released to the upper surface. Under this circumstance, the ME and WI mechanism were observed during the tests and the melt temperature decreased below the liquidus temperature of concrete (Kim et al., 2019). As a result, the termination of the ablation process occurred in some cases, i.e., CCI-2. The experimental initial conditions are incorporated as it is in MELCOR input for stand-alone simulations (section 3.1) and comparison of ablation parameters (section 3.2). For the verification study (section 3.3), initial conditions are slightly different from those of the test and are summarized in Table 4.

2.4. Simulation model of MCCI in MELCOR code

A stand-alone model has been developed using CAV package of MELCOR code (Base Code Version 2.2, Dated 17 Dec.2020 Subversion revision: 18019) to predict the ablation behavior in the CCI experiments (1–3), as shown in Fig. 3. The MELCOR requires thermal-hydraulic input incorporated through control volumes (CV) package of the code as

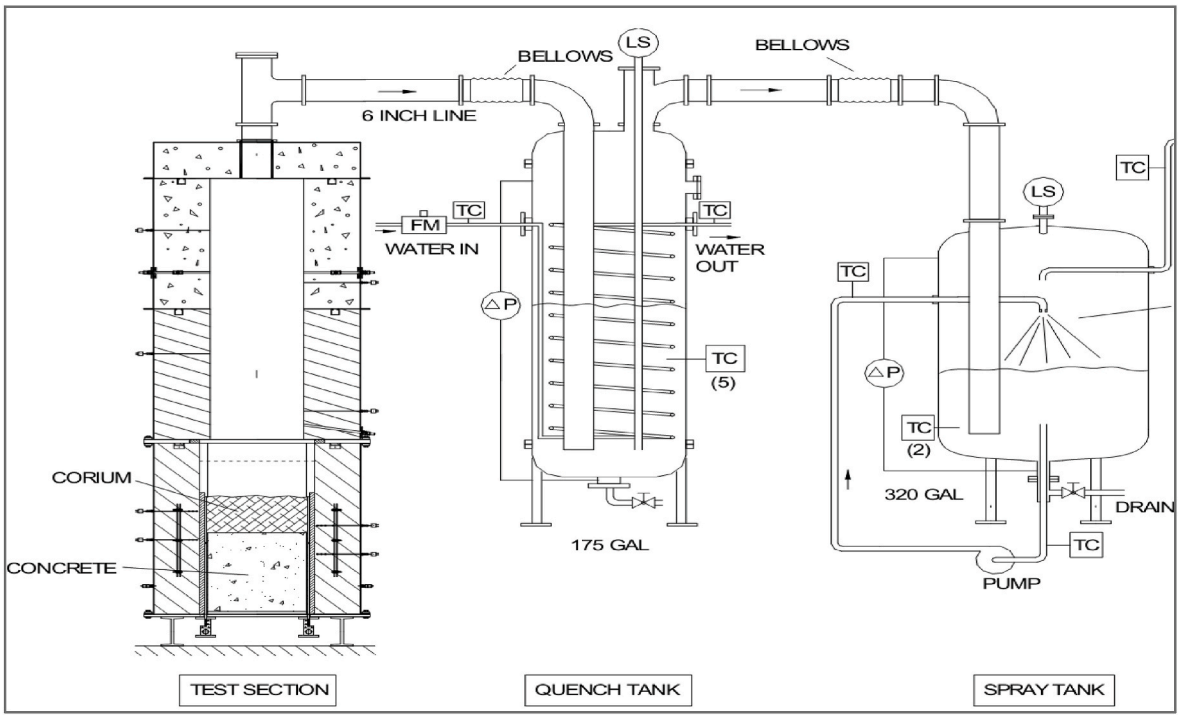

Fig. 1. Schematic diagram of CCI-2 test apparatus (Farmer et al., 2005a,b).

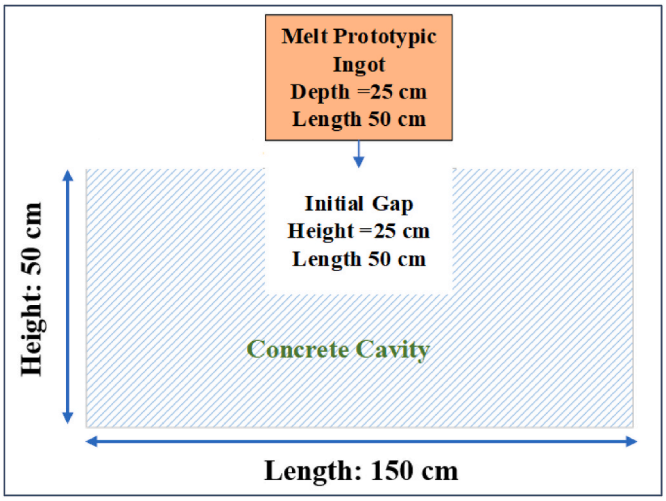

Fig. 2. Illustration of cavity concrete test section of CCI experiments and simulation.

Table 2
Test matrix and material specifications for CCI tests (Farmer et al., 2006) and simulations.

Parameter	Specification		
	CCI-1	CCI-2	CCI-3
Corium mixture	PWR with 8 wt % of SIL	PWR with 8 wt % of LCS	PWR with 15 wt % of SIL
Cavity concrete type	SIL (US-type)	LCS	SIL (EU-Type)
Basemat dimension	50 cm × 50 cm	50 cm × 50 cm	50 cm × 50 cm
Initial melt mass (depth)	400 kg (25 cm)	400 kg (25 cm)	375 kg (25 cm)
limit set for Radial and axial ablation	35/35 cm	35/35 cm	35/35 cm
System Pressure	Atmospheric	Atmospheric	Atmospheric
Temperature of water	20 °C	20 °C	20 °C
Flow rate of water	2 L/s	2 L/s	2 L/s
Melt heating technique	DEH	DEH	DEH
Power supply operation prior to water addition	Constant rate 150 kW	Constant rate 120 kW	Constant rate 150 kW
Initial temperature of melt	1950 °C	1880 °C	1950 °C

follows: the axial and radial blocks of the concrete were modeled in the crucible volume (CV-100). The crucible was connected to another volume of the experimental setup using a flow path (FL) named (FL-200). Fig. 3 shows the nodalization of MELCOR input. The heat generation for each experiment was modeled using the control function (CF-20). An external data file (EDF) was used to model the water injection at ambient conditions at a constant flow rate of 2 kg/s directly to cavity volume. The water injection does not pass through the FL-200. The flow path FL-200 remains opened for heat and mass transfer to environment during top flooding. An intermittently operated controller was used to keep the water level in the cavity volume (CV 100) at 50 cm. The CAV package requires input of concrete geometry, material properties, and sensitivity parameters.

In MELCOR code, the cavity geometry should be modeled as cylindrical shape because of code's constraint. Accordingly, the rectangular geometry of the actual experiment is converted into cylindrical geometry. The limitation is removed by taking the base surface area (0.25 m^2) and flow area (0.25 m^2) of test section in this simulation. This base area remains the same both in the experiment and simulation and this approach has already used for MCCI result comparisons of CCI tests in previous MELCOR versions (Sevon, 2017). This eases the comparison of volumetric heat generation and transfer rates in cavities.

The radial and axial ablation profiles provide only a limited amount of information about the extent of ablation behavior because MELCOR corium concrete model was originally derived from one-dimensional CORCON code (Humphries et al., 2021a). To overcome this code's limitation, ablation behavior is more appropriately described by the parameter of volume of ablated concrete (Adolf and Petr, 2010). The ablated concrete volume of CCI-2 experiment is discussed in section 3.1.2, where the comparison of concrete ablation volumes of this study

Table 3
Prototypic melt composition used in experiments (Farmer et al., 2006) and simulations.

Experiment	Constituents (Mass, kg)							Total
	UO_2	ZrO_2	SiO_2	MgO	Al_2O_3	CaO	Cr	
CCI-1	243.88	100.16	25.52	0.28	1.52	5	23.64	400.0
CCI-2	242.48	99.6	13.56	4.56	1.64	12.52	25.64	400.0
CCI-3	211.41	86.82	41.92	0.45	2.4	8.31	24.06	375.37

Table 4
Description of parameters used for the comparative analysis of CORQUENCH and MELCOR 2.2 code.

Parameter	CCI-2	CCI-3
Cavity Concrete type	SIL (US-type)	SIL (EU-Type)
Basemat cross section	50 cm × 50 cm	50 cm × 50 cm
Initial melt mass (depth)	400 kg (25 cm)	375 kg (25 cm)
Initial surface area of concrete	0.25 m^2	0.25 m^2
Solidus temperature	1393 K	1403 K
Liquidous temperature	1568 K	1523 K
Ablation temperature	1500 K	1450 K
Concrete initial temperature	293 K	293 K
Concrete emissivity	0.6	0.6
Concrete density	2330.15 kg/m^3	2340.15 kg/m^3
Decay heat rate (DEH)	101.64 kW	101.50 kW
Initial melt temperature	2153 K	2223 K
Gas Film Model bottom/side	GAS	SLAG

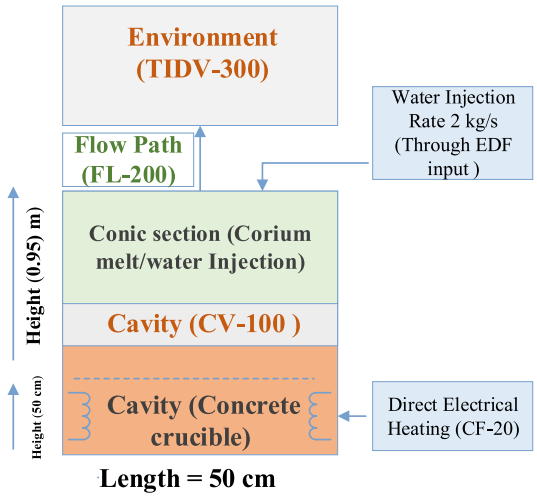

Fig. 3. Nodalization of the cavity of CCI experiments being simulated in MELCOR 2.2.

and experiment is analyzed.

There are two modeling options available for handling several layers of corium melt. The first treats metals and oxides as separate layers, which is same with modeling of CORCON Mode 2. It can calculate maximum of three layers: metal, heavy oxide underneath the metal, and light oxide above the metal. The second is a mechanistic approach, which considers the likelihood of mixing heavy oxides into metals or metals through gas flows at their interfaces (Humphries et al., 2021a). This methodology was used in present study by considering the mixing of the layers of the melt.

The WI and ME models based on the CORCON Mode 3 code are already included in the CORQUENCH code. To conduct a comparison with the CORQUENCH code, simulations of CCI-2 and CCI-3 with MELCOR code 2.2 were performed seperately as well. This analysis used another set of inputs similar to CORQUENCH study as shown in Table 5. Therefore, MELCOR model was modified before the simulation, i.e., the same concrete properties and decay heat profile as used in the reported study (Farmer, 2018).

Table 5
The values of important parameters predicted in MELCOR calculation.

Parameter	CCI-1	CCI-2	CCI-3
Important test conditions (input values)			
i. Time to achieve full DEH	90 s	90 s	90 s
ii. Decay heat DEH (120 kW)	4062 s	18100 s	6282 s
iii. Water flooding	7200 s	25000 s	10400 s
iv. Termination of test Melt Temp	1950 °C	1850 °C	1950°
Results; maximum cavity ablation			
Radial	10 cm	30 cm	17 cm
Axial	12 cm	15.4 cm	11.5 cm
Average ablation depth			
Radial	12.8 cm	20.6 cm	14.4 cm
Axial	8.5 cm	11.8 cm	8.8 cm
Water ingression and melt eruption	Not included	Activated in the code	Not included
Cavity oxidic mixture volume at the end of the simulation	0.215 m^3	0.23 m^3	0.227 m^3
Volume of the ablated concrete	0.157 m^3	0.21 m^3	0.177 m^3
Maximum cavity mass (oxidic) at the end of the simulation (including melt)	756 kg	886 kg	795 kg
Gas production	6 kg	240 kg	52 kg
Heat removal (max at water addition) from cavity surface	197 kW	933 kW	190 KW
Heat Flux (Maximum) at surface	788 kW/m^2	3732 kW/m^2	760 kW/m^2

3. Result and discussion

Section 3.1 contains the predictions of the simulations using MELCOR 2.2, which are compared with the values of each experiment. The temperaturesof the oxide layer, heat transfer rates, maximum ablation fronts in both directions, and masses of various melt concrete reaction products were included. Section 3.2 discusses the comparison of potential parameters derived from three studies. The results of the study performed in comparison with the CORQUENCH code are presented in Section 3.3.

3.1. Stand-alone simulations

3.1.1. Comparison with experimental results of CCI-1

The CCI-1 experiment was performed with siliceous (SIL) concrete with a decay power rate of 150 kW. The CCI-1 test was conducted for a short time because the cavity reached the maximum ablation depth limit (35 cm) at the southside due to asymmetric ablation in the radial direction. Therefore, water addition started at 4000 s, and data acquisition/test terminated at 7200 s. In the present study, the corium-concrete interaction observed up to 7200 s.

The corium melt has some fraction of concrete before CCI so that it has relatively higher density than light metal (steel). When further concrete is added to HMX, it becomes lighter in density and turns into light oxide mixture (LOX). Fig. 4 shows the temperatures of each layer inside the corium formed during corium-concrete reaction. The temperatures of oxidic mixture are lower than surface temperature and this trend reverses after water addition due to increased heat transfer from surface to water. The temperature measured in experiment are average of number of locations inside the corium. Oxidic mixture temperature

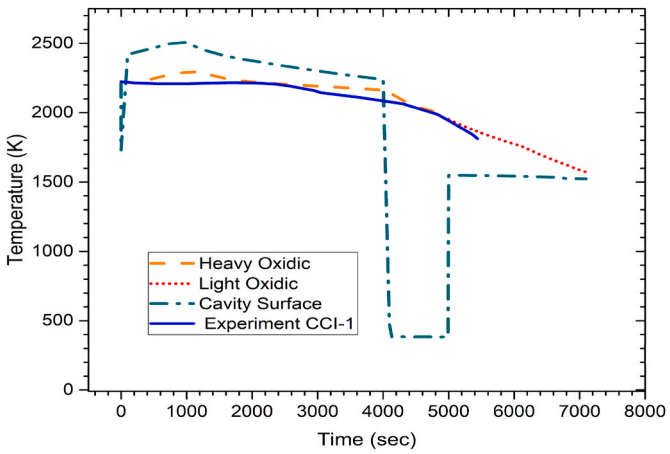

Fig. 4. Comparison between cavity surface temperature (T-SURF), average light oxidic temperature (T-LOX), average heavy oxidic temperature (T-HMX) predicted in present study and measured in CCI-1 experiment (average melt temperature).

predicted with MELCOR calculation are comparable to values of the experiment.

Fig. 5 illustrates the trends in the production of the masses of LOX, HMX, and NCG. It is confirmed that NCG generation was very low in the CCI-1 experiment. Firstly, it is because the type of concrete used (SIL) had a low carbonate content. Accordingly, small mass of gases is generated during concrete decomposition. Second, the shorter duration of the test and early water injection The LOX production rate slowdown due to decrease in melt temperature with passage of time. The CCI continued until temperature (T-LOX) (as given in Fig. 4) remained higher than the ablation temperatures.

Part of decay heat is transferred to the concrete and remaining is removed to air or overlying water. The heat transfer rates for the decay heat simulation utilizing DEH, concrete ablation, and atmosphere/water are depicted in Fig. 6. After water addition, the heat transfer to upper surface increased substantially, which reduced the melt–concrete front temperatures responsible for the ablation progression. It is noted that there were fluctuations in applied power (Direct Electrical Heating) in the experiment notably a sudden drop at 2900 s. This may be due some problem to power supply or data acquisition system. A constant (time averaged) value of DEH of 150 kW mentioned in reference (Farmer et al., 2006), (Farmer et al., 2004a,b) was used as decay heat in simulation in CCI.

Fig. 7 shows the maximum ablation depth for both directions. For the

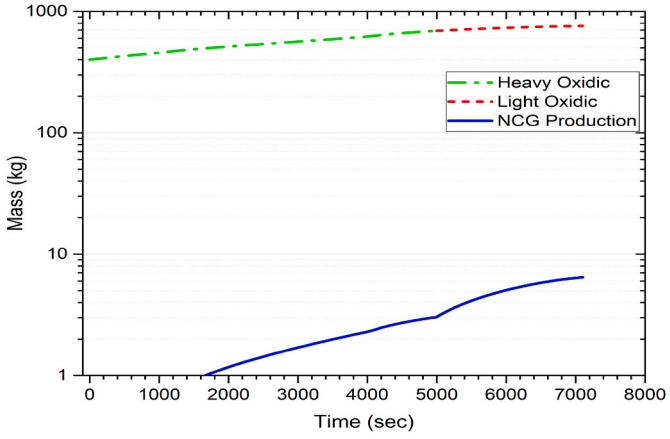

Fig. 5. MELCOR simulation results of oxidic masses (HMX, LOX) and Non-Condensable Gases (NCG) released from the cavity in CCI-1.

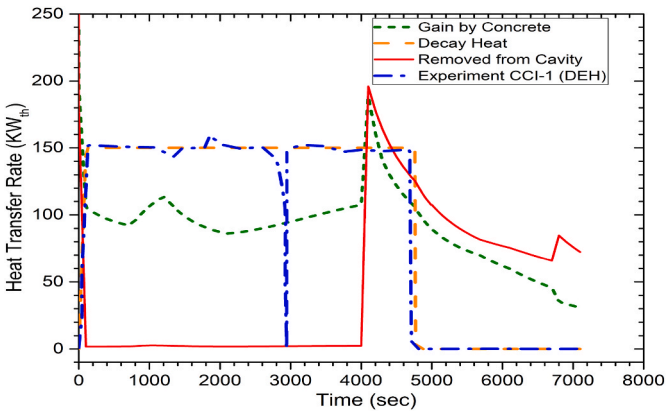

Fig. 6. MELCOR simulation results of the decay heat, heat removal rate from the cavity to the environment, heat loss to the cavity for ablation, and DEH values in CCI-1.

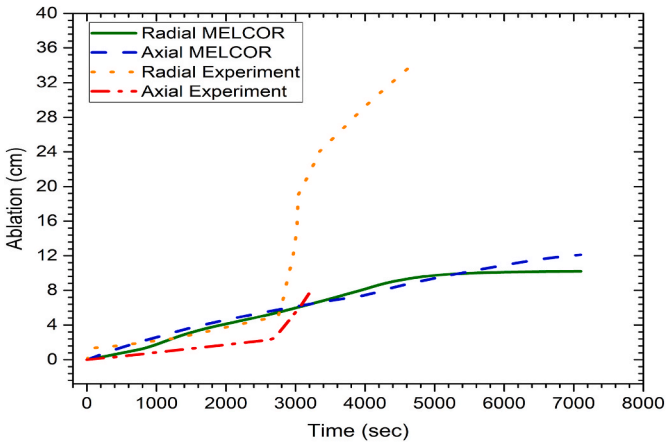

Fig. 7. The maximum ablation front predicted in CCI-1 study and experimental values (maximum ablation length in radial and axial directions).

experiment, the axial melt front attained 8 cm, whereas the radial melt front reached 35 cm. On the other hand, MELCOR predicted both ablation depths similarly, which is 12 and 10 cm, respectively. MELCOR code significantly overestimate the axial ablation and underestimate the radial ablation for the Siliceous concrete (CCI-3). This is confirmed in early simulations with MELCOR 1.8.6 and 2.1 (Sevon, 2017). The same deficiency is observed in present work using 2.2 version. Therefore, MELCOR predicts a relatively symmetrical ablation behavior. The concrete ablation volume and mass of ablated quantities, the volume of the oxide mass and the average ablation lengths in the radial/axial directions were calculated and are presented in Table 5.

3.1.2. Comparison with experimental results of CCI-2

Unlike CCI-1 experiment, CCI-2 experiment was conducted using LCS concrete, and water was injected at late stage. Fig. 8 shows the temperature behavior of corium layer and upper surface during the experiment. The average temperature of the corium measured in the experiment was higher than the temperatures of the oxidic layers predicted by MELCOR simulation. After water injection, a significant temperature difference was observed between the simulation and experimental values of LOX. The cavity surface temperature was found to be higher than the LOX temperatures after water addition. It was judged that this is due to temperature increase by erupted melt according to ME.

Fig. 9 shows the predicted temperatures for both directions of LOX layer. For axial temperature, the temperature increased after water

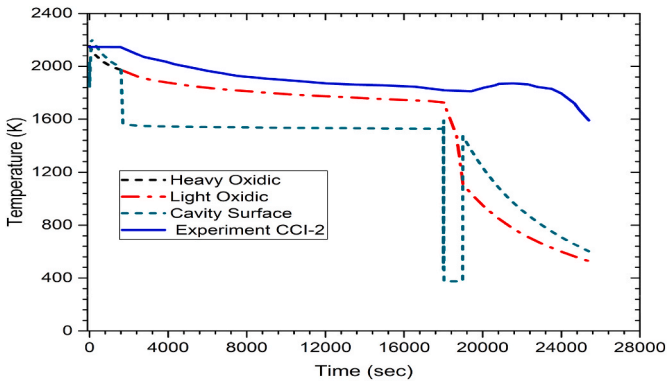

Fig. 8. Comparison of cavity surface temperature, average LOX temperature, average HOX temperature predicted by MELCOR, and average melt temperature measured in CCI-2.

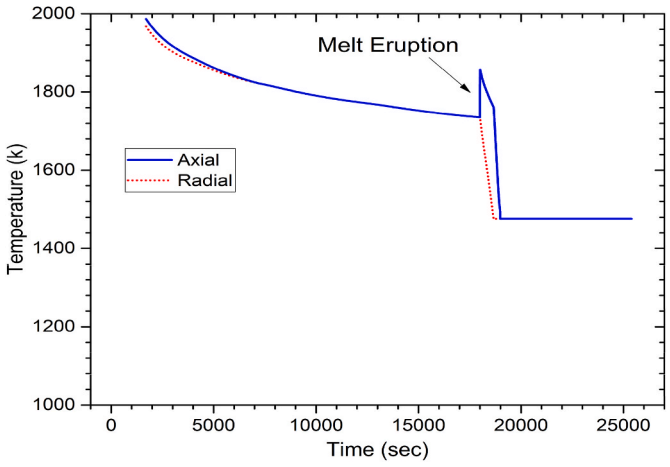

Fig. 9. Light oxidic mixture (LOX) temperature in radial and axial direction in CCI-2.

addition at 18,047 s, which was also observed in the experimental findings (Farmer et al., 2006). The heat transfer from the melt to water was significantly higher in CCI-2 than in other two experiments, as shown in Fig. 10. After the water addition, the heat transfer to water became greater than the heat transfer to the ablation process, which reduces the melt–concrete front temperatures. As a result, the ablation halts at this stage.

Fig. 11 shows the masses of HMX, LOX, and generation of NCGs. Introduction of ablated concrete into HMX layer cause the layer to turn

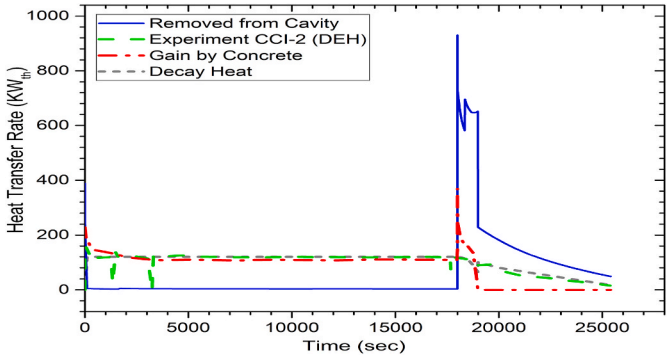

Fig. 10. MELCOR simulation results of the decay heat, heat removal rate from the cavity to the environment, heat loss to the cavity for ablation, and DEH values in CCI-2.

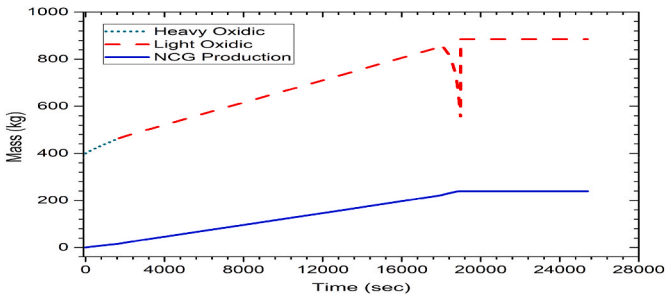

Fig. 11. MELCOR predicted oxidic masses (HMX, LOX) and NCG released from the cavity in CCI-2.

into LOX layer. It was predicted that NCGs were produced in large quantities (240 kg) in CCI-2, which results in increase in mixing and stirring of the melt-concrete mixture. After the water addition, no additional mass formation was observed because the temperature (Figs. 8 and 9) decreased below the ablation temperature/liquidus temperature of the concrete.

Fig. 12 shows the location of the melt front in both directions. The radial profile predicted was comparable to the observed in the experiment. However, the axial profile was low (15 cm) in comparison with the experimental value (29 cm). Therefore, it was necessary to compare other parameters, such as the volume or mass of the ablated mixture.

Fig. 13 shows the volume of the ablated concrete predicted by the MELCOR 2.2 code and calculated by Adolf et al. based on the experimental results (Adolf and Petr, 2010). The predicted value of the ablated concrete volume is equal to the experimental values, which is 0.21 m^3 (Adolf and Petr, 2010). Similarly, the ablated concrete mass is also very close with an error of only 0.61% as shown in Table 6.

3.1.3. Comparison with experimental results of CCI-

CCI-3 tests were conducted using siliceous concrete with constant power of 120 kW. The compositions of concrete and melt quite different with CCI-1 test. Although the tests were run longer than CCI-1, it was terminated earlier than the planned experiment time due to asymmetric ablation by reaching 35 cm of ablation depth at 10,400 s. The water addition started at 6282 s.

The temperature behavior of oxidic mixtures during the experiment and predicted with MELCOR is illustrated in Fig. 14. The temperature was noted to be lower than surface temperature at the start, but it reversed after the water addition. As a result, the surface temperature decreased below the oxide layer temperature. In this phase, the formed crust on the upper surface had a role of an insulator to avoid penetration. Therefore, small crust thickness in the axial direction facilitates better heat transfer from the cavity to the overlying water and lowers surface

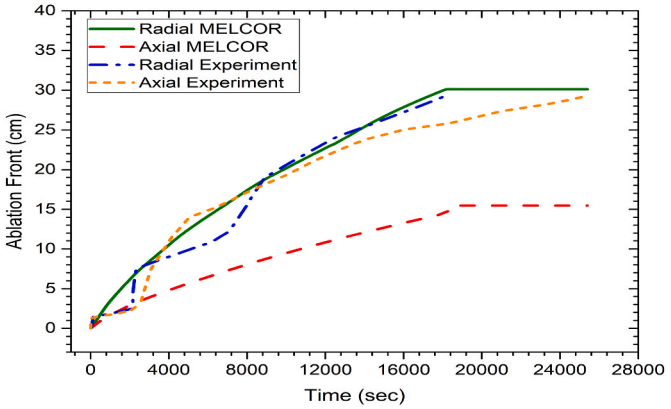

Fig. 12. The maximum ablation front predictions and experimental values (maximum ablation length in radial and axial directions) in CCI-2.

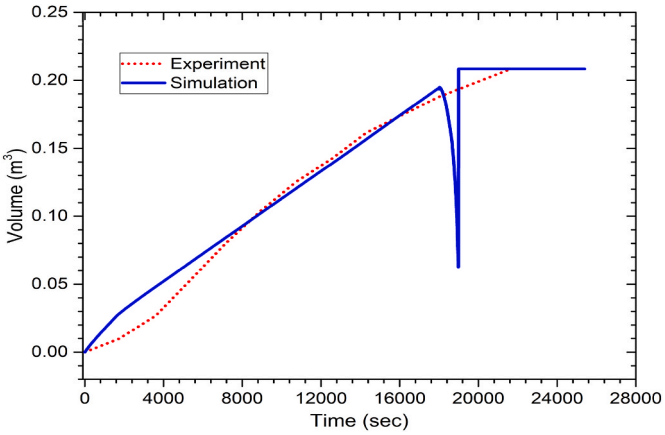

Fig. 13. Comparison of the volume of ablated concrete predicted by code and measured in CCI-2 experiment.

Table 6
Volume of concrete calculated during simulation and CCI-2 experiment.

Parameter	Simulation	Experiment (Adolf and Petr, 2010)	Difference
Volume of ablated concrete	0.21 m^3	0.21 m^3	0.0%
Density of LCS concrete	2330 kg/m^3	2330 kg/m^3	0.0%
Ablated concrete mass	486 kg	489 kg	0.62%

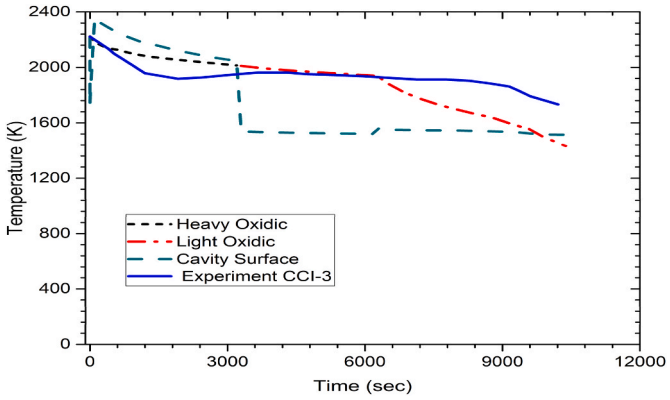

Fig. 14. Comparison of cavity surface temperature, average light oxidic temperature, average heavy oxidic temperature predicted by MELCOR, and average melt temperature measured in CCI-3.

and oxidic temperatures.

Fig. 15 illustrates the predicted trends in the production masses of LOX, HMX, and NCGs. The NCG production was predicted to be 52 kg, which is higher than that of the CCI-1 experiment because the CCI-3 test ran for a relatively longer duration. Light oxidic mixture is turned into the heavy oxidic mixture with the addition of ablated concrete. Continued mass production was observed later.

Fig. 16 shows the decay heat generation and heat removal to the atmosphere/water and concrete ablation. Despite the addition of water, heat transfer continued to the ablation process. The low crust thickness in the axial direction promoted WI and resulted in a second peak in the surface heat transfer rate. ME was not observed, which is consistent with the experimental findings because the gas content is lower in the SIL concrete used in the CCI-3 experiment.

Fig. 17 shows the comparison of maximum melt front for both directions. The experimental melt front reached 35 cm in the radial

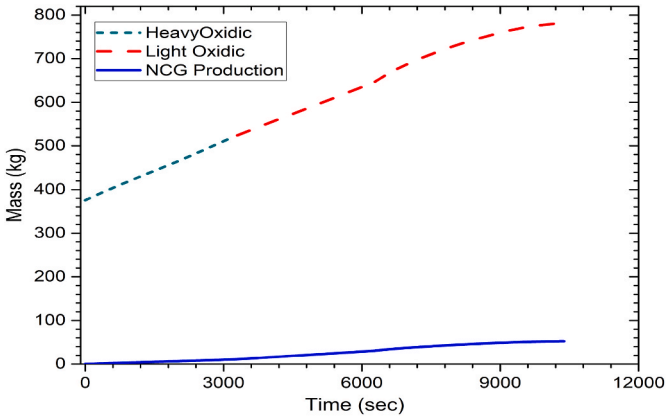

Fig. 15. MELCOR predicted oxidic masses (HMX, LOX) and NCG released from the cavity in CCI-3.

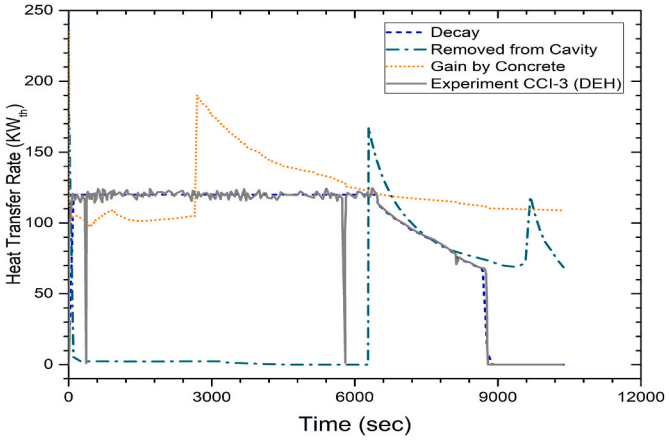

Fig. 16. MELCOR simulation results of the decay heat, heat removal rate from the cavity to the environment, heat loss to the cavity ablation, and DEH values in CCI-3.

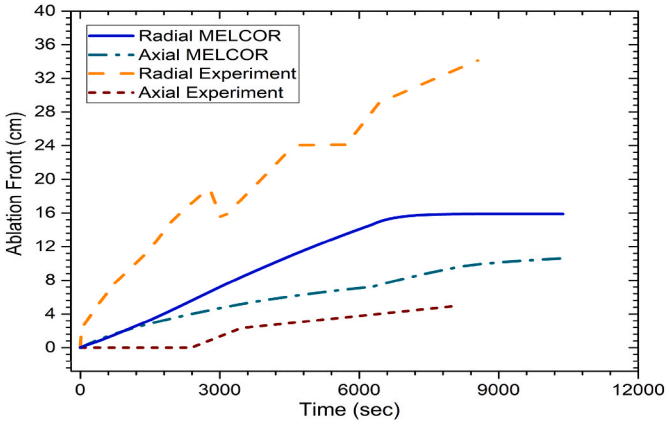

Fig. 17. The maximum ablation front predicted in CCI-3 simulations and experimental values
(maximum ablation length in radial and axial directions).

direction, whereas the MELCOR calculation predicted a value of 17 cm. For axial direction, on the other hand, the simulation predicted 10 cm, which was 5 cm greater than the experimental result. MELCOR code significantly overestimate the axial ablation and underestimate the radial ablation for the Siliceous concrete (CCI-3). This is confirmed in

early simulations with MELCOR 1.8.6 and 2.1 (Sevon, 2017). The same deficiency is observed in present work using 2.2 version.

3.2. Comparison of ablation parameters

Fig. 18 shows the predicted crust formation for both directions in MELCOR calculations for three experiments. The behavior of crust formation was different in each experiment and varied along the radial and axial directions. The oxidic phase of concrete and melt should be converted to light oxidic mixture (LOX) for crust formation (enough concrete is added in melt). Crust formation was detected in the axial direction in two instances. Firstly, the crust was observed in the initial phase of the simulations (2000–5000 s). It is because the interfacial melt is cooled by heat transfer to the concrete. However, it disappeared as soon as the crust temperature increases and reaches melting temperature. Same tendency was also observed in the CCI experiments (Farmer et al., 2006). In the later phase, crust formation was observed in the radial direction after water addition excepting CCI-2 where the axial crust thickness was approximately 12 cm. On the other hand, the thickness was quite low (1–2 cm) in CCI-1 and CCI-3.

Fig. 19 shows the predicted heat transfer rate from the melt to the concrete for each experiment. For all cases, it was confirmed that the heat transfer rate increases rapidly when the water is injected. It is because the crust are formed at the interfacial surface between melt and overlying coolant. Therefore, the remaining heat is more transferred to concrete as shown in Fig. 20. Afterward, the crust is melted so that the rate decreased gradually due to the higher heat transfer rate to upper direction, leading to the decrease of the heat transfer to concrete.

It was further noted that the present models failed to predict anisotropic ablation behavior of corium melt in the cavity and it required further improvement of models. Especially, the limitation that MELCOR CAV package only can simulates the cylindrical geometry needs to be improved to include rectangular and other geometry surfaces. The insulation of surfaces should also be included under improvement process to be able to observe the effect of insulation during ablation process.

3.3. Comparative study of CCI predictions with CORQUENCH prediction results

A comparison of the MELCOR code 2.2 calculation results for CCI-2 and CCI-3 experiments with a previous study conducted with CORQUENCH 4.1 code was conducted. To simulate same CCI situation in CORQUENCH code input (Farmer, 2018), the input model was modified before simulation in the MELCOR code such as concrete properties and decay heat as shown in Table 4. For CCI-2 and CCI-3 tests, MELCOR calculation of three cases were conducted to evaluate the effects of WI and ME models as summarized in Table 7.

Fig. 21 shows a comparison of the cavity surface heat flux predicted with MELCOR and CORQUENCH codes. The MELCOR results

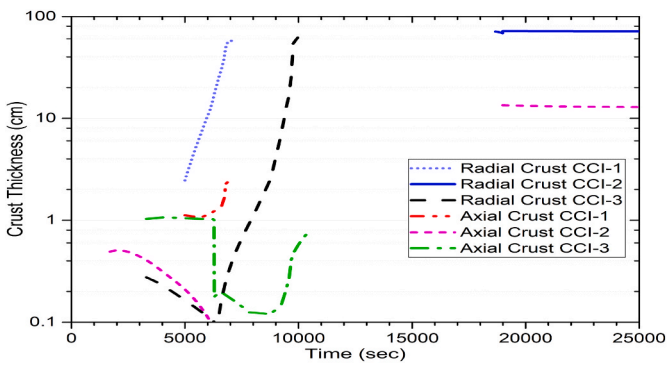

Fig. 18. Crust thickness formation above oxidic layer mixture in radial and axial directions.

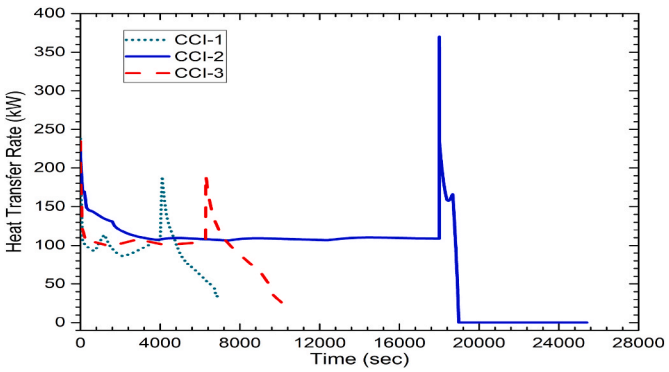

Fig. 19. Heat transfer rate to the cavity concrete for core-concrete interaction.

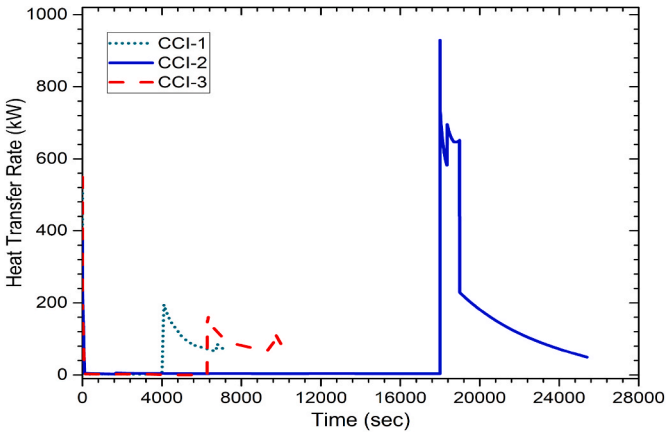

Fig. 20. Heat removal rate through the upper surface of the cavity to atmosphere and water pool in case of top flooding.

Table 7
MELCOR simulation cases for comparison with CORQUENCH calculation results.

MELCOR Case Studies	Water Ingression Model	Melt Eruption Model
With ME & WI	Active	active
With WI	Active	No
Without WI & ME	No	No

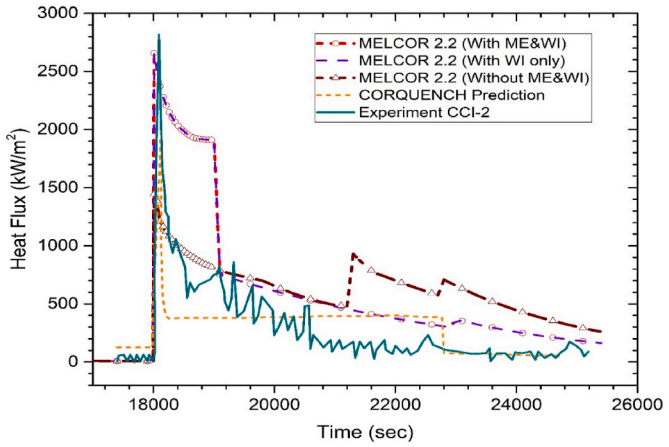

Fig. 21. Heat flux (kW/m^2) from the surface of the cavity predicted with MELCOR 2.2, CORQUENCH, and measured in CCI-2.

approximately match the experimental results when both WI and ME models are applied. It also showed a large deviation from the experiment and the CORQUENCH results (Farmer, 2018) at a late stage. MELCOR predicted a very small difference in the peak values with and without ME. The WI was active in both cases. The termination of the ablation progression for LCS concrete was possible with WI alone. The MELCOR case study without WI and ME for the CCI-2 experiment showed significantly lower heat transfer from the surface of the water in comparison with other MELCOR cases and CORQUENCH simulations.

Fig. 22 shows a comparison of the cavity surface heat flux predicted using MELCOR 2.2, CORQUENCH and measured in the CCI-3 experiment. The predicted values with MELCOR were relatively close to each other in the three case studies compared to the. The MELCOR with ME and WI predicted lower peak heat fluxes than CORQUENCH at the water injection stage and higher at later stages for CCI-3.

Fig. 23 shows a comparison of the ablation front head (cm) in both directions predicted with MELCOR 2.2, CORQUENCH, and measured in the CCI-2 experiment. The comparison shows similar trends in the radial direction; however, MELCOR 2.2 predicted a lower ablation front head in the axial direction, and the details are discussed in Section 3.1.1.

Fig. 24 presents a comparison of the ablation front head (cm) in the radial and axial directions of the cavity predicted with MELCOR 2.2, CORQUENCH, and measured in the CCI-3 experiment. Asymmetric ablation in the radial direction was observed in the experiment and CORQUENCH calculation (Farmer, 2018). MELCOR predicted higher values in the axial direction and lowest values in the radial direction in comparison to the experiment and CORQUENCH prediction.

The MELCOR code CCI prediction could be seen in the comparison of some previous studies as follows:

In the study by Kim et al. (2005), scaling criteria were applied to determine the comparable cylindrical geometry but this requires a variable heating rate different than used in experiment. It was taken care off to have same volume ratio of molten concrete and melt, initial heat flux and area ratio of the bottom/side wall.

A sensitivity analysis (Jung et al., 2018) is performed for CCI-2 and CCI-3 experiments with MELCOR 2.2 using the scaling approach (Kim et al., 2005). It is noted that the heat fluxes and ablation profiles are affected by the variation in the input parameters (heat transfer mechanisms and concrete properties).

In another study by Cho et al. (2020), uncertainty analysis of input parameters needed in MECOR 1.8.5 to 2.2 is performed for CCI-2. The study shows a large variation in position of the axial and radial ablation front when input parameters are changed. The comparison of the ablation front positions determined in the present study with the previous studies (Kim et al., 2005), (Jung et al., 2018), (Cho et al., 2020) is presented in Table 8. The ablation front position predicted by the present study is comparable with that of other studies. It is also noted that the input parameters/code options, selected for simulation have a strong effect on the predicted values.

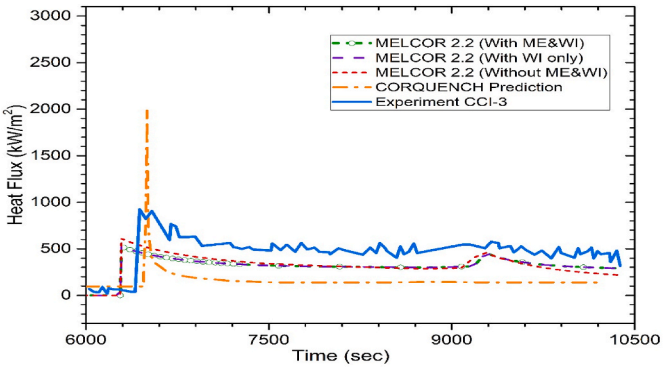

Fig. 22. Heat flux (kW/m^2) from the surface of cavity predicted using MELCOR 2.2, CORQUENCH and measured in CCI-3 experiment.

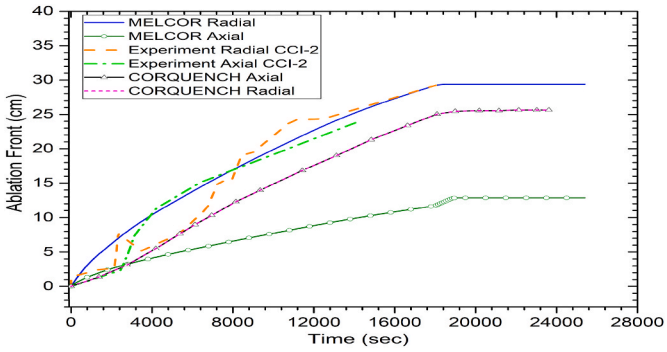

Fig. 23. Comparison of ablation front head (cm) in radial and axial directions of the cavity predicted with MELCOR 2.2, CORQUENCH, and measured in CCI-2.

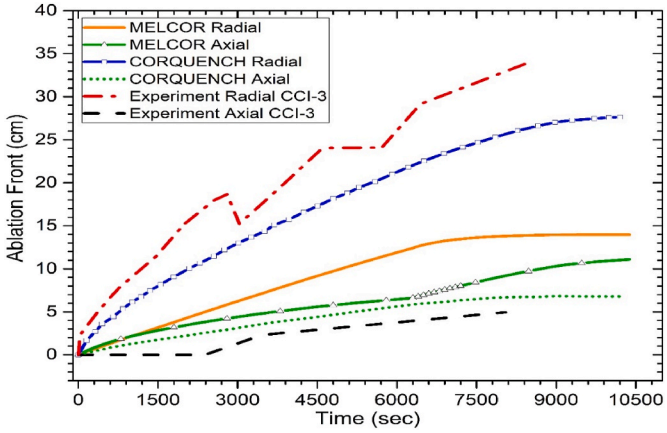

Fig. 24. Comparison of ablation front head (cm) in radial and axial directions of the cavity predicted with MELCOR 2.2, CORQUENCH, and measured in CCI-3 experiment.

Table 8
Comparison of the ablation front positions (cm) determined in the present study with the previous studies.

Sr. No.	Technique	CCI-2		CCI-3	
		Axial	Radial (North)	Axial	Radial (North)
1	Experimental (Farmer et al., 2006)	25	30	6	34
2	MELCOR 2.2 sensitivity analysis (Jung et al., 2018)	30	42.5	10	32.5
3	CCI Uncertainty analysis MELCOR parameters 1.8.5 to 2.2 (Cho et al., 2020)	20–32	14–35	–	–
4	MELCOR 2.2 (Current study)	30	13	11	14
5	CORQUENCH (Farmer, 2018)	25	25	6	27

The validation and verification of this MELCOR model with CORQUENCH is satisfactory and it can be used for real reactor applications. In the future research work, the studies can be performed to investigate the MCCI under top flooding for a Small Modular Reactor (SMR). The study will be helpful to further strengthen the accident management procedure during late phase of severe accident to improved reactor safety (Hengra et al., 2023). The appropriate type of cavity concrete and effect of delayed water injection under top flooding will be the key factor for successful termination of CCI for SMR.

There exist several modeling differences in MELCOR and CORQUENCH in predicting WI, ME and physical properties estimation i.e.,

thermal conductivity, viscosity and solidus temperatures of corium concrete mixture at the interface. The geometric and modeling approach differences should be addressed in the future versions of both codes. The ME is important for LCS concretes (as used in CCI-2 test). Water is added in delayed stage in CCI-2 test resulting in competing effects of WI and ME along with lowering of mixture temperatures (below liquidous temperatures) during MCCI process. The CCI-2 experiment did not provide clear evidence of effectiveness of these phenomena. Future experimental studies need to be performed with early cavity flooding for different concrete types especially having enough carbonaceous content. The effect of oxidation of corium mixture is not well addressed in the CCI 1–3 experiments. It is important for real reactor corium masses which are partially oxidized. The quantification of the mass entrainment by ME and lowering of liquidous temperatures could be ascertained by further research in this area. It is suggested to include more detailed mechanistic physical models of WI and ME in MELCOR. These types of models are implemented in CORQUENCH and MELT SPREAD codes. The present melt eruption model in MELCOR requires further improvement to include the impact of cooling in the absence of gas bubbling (as it required sufficient gas entrainment) (Farmer et al., 2010).

4. Summary and conclusion

In this study, an investigation was conducted to evaluate the effectiveness of the top flooding strategy in stabilizing the melt, and the ablation front, temperature, and heat transfer of different concrete types under dry conditions were evaluated. Additionally, the termination of the ablation progression using the top flooding approach was examined. To evaluate and assess the improvements made to the MELCOR 2.2 code, simulations were performed for the CCI-1 to CCI-3 experiments. SIL concrete with decaying powers of 150 kW and 120 kW was used for CCI-1 and CCI-3 studies, respectively, while LCS concrete with a decay heat rate of 120 kW was used for the CCI-2 experiment, in which water injection occurred at a later stage. Another study was conducted to compare the results of CORQUENCH and MELCOR 2.2 under similar conditions. The key findings of this study are summarized as follows:

i. The ablation progression was successfully terminated in the case of LCS concrete (CCI-2 experiments) through the use of water ingression and melt eruption models in MELCOR simulations, which reduced cavity temperatures below the liquidus temperatures of the cavity.
ii. MELCOR simulations of the CCI-1 to CCI-3 experiments showed maximum and average melt front values in agreement with experimental results, while CCI-2 exhibited symmetric ablation progression in contrast to the experiment's asymmetric ablation.
iii. The ablated volume and mass of concrete in the CCI-2 experiment showed excellent agreement between MELCOR 2.2 prediction and experimental data. MELCOR simulations did not predict exponential and anisotropic ablation in a particular direction, as observed in experiments. Instead, gradual rise in the ablation melt front was noted in all case studies.
iv. The MELCOR CAV package currently only allows for simulation of cylindrical geometry and requires improvement to include rectangular and other geometry types.
v. To account for the effect of insulation of particular surfaces, the MELCOR code cavity package should include insulation of surfaces.
vi. A shift from parametric to mechanistic modeling approach may improve the code predictions. Mechanistic models for the water ingression and melt eruption phenomena should be employed in MELCOR code.
vii. Future experimental studies should investigate the effect of corium oxidation in conjunction with early flooding of the cavity.
viii. The separate effects of reduction of solidus temperature by addition of concrete in the mixture and through water ingression and melt eruption cannot be studied independently in the code, and it needs improvement to include separate effect investigation options for these phenomena.

Declaration of competing interest

A research paper on "**Parametric study of molten core concrete interaction and assessment of corium coolability in context of MCCI experiments**" is being submitted in the international journal "Progress in Nuclear Energy". It is stated that the authors have no conflict of interest with the reviewers and the editors.

Data availability

Data will be made available on request.

Acknowledgments

This research has no funding source. The computational resources provided by Hanyang University. Pakistan's Higher Education Commission (HEC) also partially supported for travelling and living expenses.

References

Adolf, R., Petr, V., 2010. An attempt to model the heat conduction in concrete during CCI: simulation of the CCI-2 test with CORCON in MELCOR. In: EMUG Meeting. NRIR, Prague, Czech Republic.
Alsmeyer, H., Adelhelm, C., Dilmann, G.H., Foit, J., et al., 1995. BETA experiments on melt - concrete interaction: the role of zirconium and the potential sump water during core melt-down accidents. Nucl. Eng. Des. 154 (1), 61–68.
Amidu, M.A., Addad, Y., 2022. The influence of the water ingression and melt eruption model on the MELCOR code prediction of molten corium-concrete interaction in the APR-1400 reactor cavity. Nucl. Eng. Technol. 54, 1508–1515. https://doi.org/10.1016/j.net.2021.09.036.
Blose, R., Brockmann, J., Copus, E., Powers, D., et al., 1993. Core-Concrete Interactions with Overlying Water Pools: the WETCOR-1 Test. Sandia National Laboratories, Albuquerque.
Bradley, D., Gardner, D., Brockman, J., et al., 1993. CORCON-MOD3: an Integrated Computer Model for Analysis of Molten Core-Concrete Interactions. Userís Manual., Albuquerque, USA.
Cai, Q., Zhu, D., Chen, R., et al., 2020a. hree-dimensional numerical study on the effect of sidewall crust thermal resistance on transient MCCI by improved MPS method. Ann. Nucl. Energy 144, 107525.
Cai, Q., Zhu, D., Chen, R., et al., 2020b. Three-dimensional numerical study on the effect of sidewall crust thermal resistance on transient MCCI by improved MPS method. Ann. Nucl. Energy 144, 107525.
Chai, P., Kondo, M., Erkan, N., et al., 2017. Numerical simulation of MCCI based on MPS method with different types of concrete. Ann. Nucl. Energy 103, 227–237.
Cho, Y.J., Lee, Y., Lim, K., Ha, S.-k., 2020. Statistical treatment of MELCOR uncertainty study of CCI2 using Dakota/SNAP. In: Transactions of the Korean Nuclear Society Virtual Spring Meeting. Vitual Meeting.
Christophe, j., Eric, B., Jean, M.B., et al., 2010. European experiments on 2-D molten core concrete interaction: HECLA and VULCANO. Nucl. Technol. 170 (1), 189–200.
Eppinger, B., Fellmoser, F., Fieg, G., Massier, H., Stern, G., 2000. Experiments on Concrete Erosion by a Corium Melt in the EPR Reactor Cavity: KAPOOL 6-8. Karlsruhe: Forschungszentrum Karlsruhe, p. 32 (FZKA 6453.).
Epstein, M., 2006. Dryout heat flux during penetration of water into solidifying rock. J. Heat Tran. 128 (8), 847–850.
Farmer, M., 2017. The MELTSPREAD Code for Modeling of Ex-Vessel Core Debris Spreading Behavior. Nuclear Engineering Division, Argonne National Laboratory, Argonne, Illinois, USA.
Farmer, M.T., 2018. The CORQUENCH code for modeling of ex-vessel corium coolability under top flooding conditions; code manual –Version4.1-beta. In: Nuclear Science and Engineering Division, Argonne National Laboratory. Code Manual, Version4.1-beta, p. 222.
Farmer, M.T., Spencer, B.W., Binder, J.L., Hill, D.J., 2001. Status and future direction of the melt attack and coolability experiments (MACE) program at Argonne National Laboratory.. United States. In: 9th International Conference on Nuclear Engineering (ICONE-9). Nice (FR), 04/08/2001–04/12/2001.
Farmer, M.T., Lomperski, S., Kilsdonk, D.J., Aeschlimnann, R.W., 2004a. CCI-1 Test Data Report-Thermalhydraulic Results, OECD/MCCI-2004-TR01. Nuclear Engineering Division, Argonne National Laboratory, Albuquerque, USA.
Farmer, M.T., Lomperski, S., Kilsdonk, D.J., Aeschlimann, R.W., 2004b. CCI-2 Test Data Report-Thermalhydraulic Results. Nuclear Engineering Division, Argonne National Laboratory, USA., Argonne, IL 60439 USA.

Farmer, M., Lomperski, S., Steve, W., Basu, S., 2005a. The Results of the CCI-2 Reactor Material Experiment Investigating 2-D Core-Concrete Interaction and Debris Coolability. Argonne, IL 60439 USA.
Farmer, M.T., Lomperski, S., Kilsdonk, D.J., 2005b. CCI-3 Test Data Report-Thermalhydraulic Results. Argonne, IL 60439 USA.
Farmer, M.T., Lomperski, S., Kilsdonk, D.J., Aeschlimann, R.W., 2006. OECD MCCI Project 2-D Concrete Interaction (CCI) Tests: Final Report. Argonne, IL 60439 USA.
Farmer, M.T., Kilsdonk, D.J., Aeschlimann, R.W., 2009. Corium coolability under ex-vessel accident conditions for LWRs. Nucl. Eng. Technol. 41, 575–602.
Farmer, M.T., Lomperski, S., Aeschlimann, W.R., Kilsdonk, D.J., 2010. OECD MCCI Project Category 2 Coolability Engineering Enhancement Tests. Argonne, IL 60439 USA.
Greene, G.A., 1991. Heat, mass, and momentum transfer in a multifluid bubbling pool. Adv. Heat Tran. 21, 277–346.
Hengra, N.H., Song, C.H., Kim, S.J., Ilyas, M., 2023. Assessment of corium concrete interaction and impact of water ingression mechanism using top flooding strategy for a small PWR with MELCOR 2.2. Ann. Nucl. Energy 182, 109601.
Huber, F., Albrecht, G., Jenes, E., Sch, W.t., 2005. KAJET Experiments on Pressure-Driven Melt Jets and Their Interaction with Concrete. Forschungszentrum Karlsruhe., Karlsruhe.
Humphries, L., Phillips, J., Schmidt, R., Brad, B., Wagner, K.C., Louie, D., 2019. MELCOR Code Change History Revision 11932 to 14746. Albuquerque,USA.
Humphries, L.L., Beeny, B.A., Gelbard, F., Haskin, T., et al., 2021a. MELCOR Computer Code Manuals, vol. 1. Primer and User's Guide.
Humphries, L.L., Beeny, B.A., Gelbard, F., et al., 2021b. "MELCOR computer code manuals. Reference Manual 2. SAND2021-0241.
Incropera, F., DeWitt, 2002. Fundamentals of Heat and Mass Transfer, 5Th ed. John Wiley & Sons, Hoboken, NJ, p. 981.
Journeau, C., Bouyer, V., Cassiaut-Louis, N., Fouquart, P., Piluso, P., et al., 2018. Safest roadmap for corium experimental research in europe. ASCE-ASME J. Risk Uncertain. Eng. Syst. Part B Mech. Eng. 4, 30901–30910.
Jung, W.H., Hwang, B., Park, S.H., Moriyama, K., 2018. Simulation of CCI experiments for the sensitivity analysis with MELCOR 2.2. In: Transactions of the Korean Nuclear Society Autumn Meeting. Yeosu, Korea.
Kevin, R.R., Matthew, W.F., Farmer, M.T., 2014. Ex-Vessel Core Melt Modeling Comparison between MELTSPREAD-CORQUENCH and MELCOR 2.1. Oak Ridge, USA. Tennessee 37831–6283.
Kim, J.H., Kwon, S., Choi, J., Cho, Y.J., 2019. Concrete ablation analysis for molten corium-concrete interaction mitigation strategy. Ann. Nucl. Energy 132, 615–627. https://doi.org/10.1016/j.anucene.2019.06.057.
Kim, H.Y., Song, J.H., Kim, H.D., 2005. Calculations of core concrete interaction using MELCOR 1.8.5. In: Proceedings of the Korean Nuclear Society Conference. South Korea.
Li, X., Yamaji, A., 2016. A numerical study of isotropic and anisotropic ablation in MCCI by MPS method. Prog. Nucl. Energy 90, 46–57.
Li, G., Liu, M., Wang, J., et al., 2017. Crust behavior and erosion rate prediction of EPR sacrificial material impinged by core melt jet. Nucl. Eng. Des. 314, 44–55.
Lomperski, S., Farmer, M., 2007. Experimental evaluation of the water ingression mechanism for corium cooling. Nucl. Eng. Des. 237, 905–917.
Nayak, A.K., Singh, R.K., kulkarni, P.P., Sehgal, B.R., 2009. A numerical and experimental study of water ingression phenomena in melt pool coolability. Nucl. Eng. Des. 239, 1285–1293.
Penghui, C., Masahiro, K., Nejdet, E., Koji, O., 2017. Numerical simulation of MCCI based on MPS method with different types of concrete. Ann. Nucl. Energy 103, 227–237.
Sevon, T., 2005. Molten Core - Concrete Interactions in Nuclear Accidents. VTT Technical Research Centre of Finland. Vuorimiehentie 5, P.O.Box 2000, FI–02044 VTT, Finland.
Sevon, T., 2017. Modeling of water ingression mechanism for corium. Nucl. Technol. 197 (2), 171–179.
Xu, Z., Zhang, Y., et al., 2022. Experimental study on molten corium-concrete interaction with simulant metal and oxide. Ann. Nucl. Energy 167, 108767.
Yeo, D.Y., 2018. Effects of Porous Media on Heat Removal Capability during Normal and Severe Accident Conditions of PWR.
Yeo, D.Y., No, H.C., 2019. Modeling crust fracture and water ingression through crust during top-flooding strategy for corium cooling. Nucl. Eng. Des. 219–230.

Glossary

CAV: Cavity
CCI: Corium Concrete Interaction
CV: Control volume
DAS: Data Acquisition System
DEH: Direct Electrical Heating
EDF: External Data File
HMX: Concrete-melt Heavy mixture
HOX: Concrete-melt Heavy oxidic mixture
LOX: Concrete-melt Light oxidic mixture
LCS: Limestone Common Sand
LWR: Light Water Reactor
MCCI: Molten Corium Concrete Interaction
RPV: Reactor Pressure Vessel
SIL: Siliceous (Concrete type)

Nomenclature

C_p: Specific heat capacity at constant pressure(J/kg-K)
E: Young's Modulus (Pa)
K: Thermal conductivity (J/m-K)
T: Temperature (K)
g: Gravitational acceleration (9.8 m/s^2)
j: Superficial velocity (m/s)
E_{ent}: Entrainment constant (default value 0.06)
h_{lv}: Heat transfer coefficient (W/m^2-K) for water
j_g: Volumetric gas flux / area = superficial gas velocity (m/s)
∇e_{sat}: Change in specific enthalpy from melt temperatures to saturation temperature (J/kg)
k_{ent}: Entrainment coefficient calculated from the Ricou-Spalding correlation
k_{prm}: Curst permeability (kg/Pa-m)
N_{dry}: Numerical constant (0.1 $K\text{-}m^{1/2}$)
Nu: Nusselt number
Pr: Prandtl number
q''_{dry}: Dry out heat flux (W/m^2)
Ra: Rayleigh number

Greek letters

α: Coefficient of thermal expansion for melt (1/K)
ρ: Density (Kg/m^3)
μ: Dynamic viscosity of the melt (Pa·s)
ν: Kinematic viscosity (m^2/s^{-1})
δ: Thickness (m)
σ: Tensile strength (Pa)

Subscripts

p: Pressure
cond: Conduction
cr: Crust
dry: Dry out
ent: Entrainment
g: Gas
l: Liquid/water
m: Mean/average of melt and concrete
melt: Melt/corium
sat: Saturation
T: Temperature
tens: Tensile
v: Steam /water
B: Bottom surface
S: Surface